Provided for non-commercial research and education use.
Not for reproduction, distribution or commercial use.

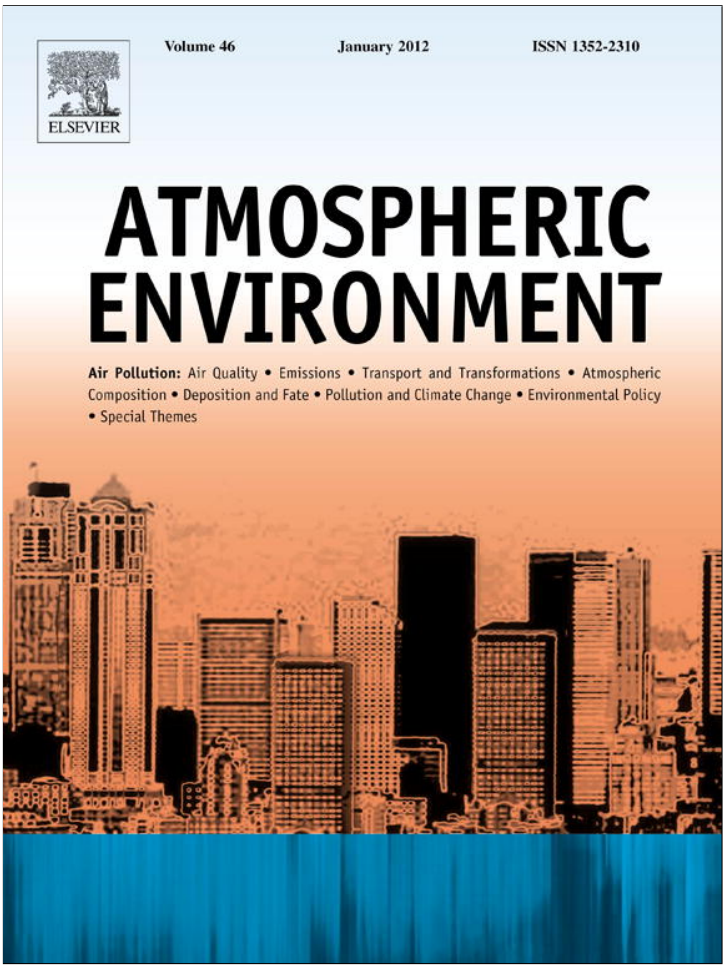

This article appeared in a journal published by Elsevier. The attached copy is furnished to the author for internal non-commercial research and education use, including for instruction at the authors institution and sharing with colleagues.

Other uses, including reproduction and distribution, or selling or licensing copies, or posting to personal, institutional or third party websites are prohibited.

In most cases authors are permitted to post their version of the article (e.g. in Word or Tex form) to their personal website or institutional repository. Authors requiring further information regarding Elsevier's archiving and manuscript policies are encouraged to visit:

http://www.elsevier.com/authorsrights

Author's personal copy

Atmospheric Environment 74 (2013) 182–193

Contents lists available at SciVerse ScienceDirect

Atmospheric Environment

journal homepage: www.elsevier.com/locate/atmosenv

Assessment of heavy metal contamination of dustfall in northern China from integrated chemical and magnetic investigation

Qingqing Qiao [a,b], Baochun Huang [b,c,*], Chunxia Zhang [b,d], John D.A. Piper [e], Yuepeng Pan [f], Ying Sun [g]

[a] Xinjiang Research Center for Mineral Resources, Xinjiang Institute of Ecology and Geography, Chinese Academy of Sciences, Urumqi 830011, China
[b] State Key Laboratory of Lithospheric Evolution, Institute of Geology and Geophysics, Chinese Academy of Sciences, Beijing 100029, China
[c] Key Laboratory of Orogenic Belt of Crustal Evolution Ministry of Education, School of Earth and Space Sciences, Peking University, Beijing 100871, China
[d] Key Laboratory of Cenozoic Geology and Environment, Institute of Geology and Geophysics, Chinese Academy of Sciences, Beijing 100029, China
[e] Geomagnetism Laboratory, Department of Earth and Ocean Sciences, University of Liverpool, Liverpool L69 7ZE, UK
[f] State Key Laboratory of Atmospheric Boundary Layer Physics and Atmospheric Chemistry, Institute of Atmospheric Physics, Chinese Academy of Sciences, Beijing 100029, China
[g] Department of Chemistry, Analytical and Testing Center, Capital Normal University, China

HIGHLIGHTS

- Magnetic properties and heavy metals in atmospheric particulate matter were compared in different regions.
- The atmospheric particulate is contaminated by local anthropogenic activity.
- Magnetic parameters can be used as a practical tool for mapping degrees of heavy metal pollution.

ARTICLE INFO

Article history:
Received 29 September 2012
Received in revised form
18 March 2013
Accepted 20 March 2013

Keywords:
Environmental magnetism
Dustfall
Heavy metals
Anthropogenic activities
Northern China

ABSTRACT

Magnetic phases are a common component of dustfall samples and mineral magnetic studies have been increasingly exploited for air quality studies in recent years to assess the source and spatial-temporal distribution of anthropogenic magnetic particulates and associated heavy metals. Here we report a comparative study of magnetic and chemical properties of atmospheric particulate deposits from rural areas of Inner Mongolia and urban regions of Hebei and Beijing. The sample sets were collected at 13 monitoring stations by the gravimetric method between April 2009 and March 2010. At the rural sites paramagnetic clays, complemented by hematite and goethite recognized by Isothermal Remanent Magnetism (IRM) and Diffuse Reflectance Spectra (DRS) investigations, accompany fine grained magnetite as an important fraction. Although present as a residual phase in samples from the urban regions, coarse-grained magnetite of anthropogenic origin dominants the magnetic signatures in these latter environments. Systematic variations with local anthropogenic activity including traffic, the mining of ores and a range of industrial emissions are identified, together with a seasonal signature in the Beijing area. We use correlations between magnetic concentration-related parameters, notably magnetic susceptibility, and the Pollution Load Index to demonstrate how magnetic parameters can be used as a practical tool for mapping degrees of heavy metal pollution and tracing the sources of pollutants in dustfall samples.

© 2013 Elsevier Ltd. All rights reserved.

1. Introduction

Atmospheric Particulate Matter (APM) exists in different forms, ranging from sub-micron aerosols to visible dust particles (Bell and Treshow, 2002). It plays an important, but detrimental, role in everyday life and influences a number of atmospheric processes (Othmar, 1996) with particle sizes <2.5 μm associated with bronchitis, cardiopulmonary and lung cancer mortality (Morris et al., 1995; Farmer, 1997). In the ecological environment APM deposition suppresses plant growth by blocking plant cores and

* Corresponding author. Key Laboratory of Orogenic Belt of Crustal Evolution Ministry of Education, School of Earth and Space Sciences, Peking University, No. 5 Yiheyuan Road, Haidian District, Beijing 100871, China. Tel.: +86 10 62755189.
E-mail addresses: qqqiaon@gmail.com, qqqiao@mail.igcas.ac.cn (Q. Qiao), bchuang@pku.edu.cn (B. Huang).

1352-2310/$ – see front matter © 2013 Elsevier Ltd. All rights reserved.
http://dx.doi.org/10.1016/j.atmosenv.2013.03.039

Author's personal copy

disrupting photosynthesis (Choi et al., 2008), and is one of the most important contributors to environmental stress (e.g. Petrovský and Ellwood, 1999).

APM typically comprises a complex mixture of different elements and compounds (Dallarosa et al., 2008) with heavy metal content particularly significant due to its toxicity and harmful effects on health. Dust containing heavy metals is dispersed globally by atmospheric circulation and becomes a minor but potent component of sediment, soils, and the hydrosphere with a major impact on Earth ecosystems (Petrovský and Ellwood, 1999). Fortunately heavy metals can be readily detected (Xia et al., 2008; Sagnotti et al., 2009) to frame policies for reducing emissions and monitoring their long-term effectiveness (e.g. Shu et al., 2001).

The methods for monitoring emissions of APM are multidisciplinary and include geochemical, mineralogical and microstructural. Since APM is emitted both from natural sources such as deserts and bared soils (Choi et al., 2001; Fang et al., 2002; Zhang et al., 2010b) and from anthropogenic processes (Xia et al., 2008; Qiao et al., 2011; Zhang et al., 2011, 2012b), a challenge to these investigations is to separate contributions from the two primary causes. In urban areas the diversity of possible anthropogenic emissions renders source assignation difficult (Choi et al., 2001; Kim et al., 2008; Zhang et al., 2012b). Although many investigations show that geochemical methods are useful for detecting APM sources (Wang et al., 2005; Kim et al., 2007), they are time-consuming and expensive. Magnetic methods provide an effective means of source ascription in air quality studies (e.g. McIntosh et al., 2007; Halsall et al., 2008) since they can be quickly and cheaply repeated many times; they provide the obvious means for monitoring regional distributions of APM and gauging temporal and spatial variations (Verosub and Roberts, 1995).

In addition to the concise association between magnetic properties of APM and heavy metal concentrations (e.g. Linton et al., 1980; Hunt et al., 1984; Beckwith et al., 1986; de Miguel et al., 1997; Xie et al., 2001; Maher et al., 2008; Zhang et al., 2011, 2012b), there is a more multi-facetted link to organic content (Xie et al., 2000) and mutagenic organic compounds (Morris et al., 1995). In this case correlations between magnetic properties and metal concentration can provide complementary information about chemical speciation; examples have been reported from single emission sites over short time scales (e.g. Xie et al., 2001; Maher et al., 2008; Zhang et al., 2011, 2012b). However, the potential use of magnetic measurement in conjunction with a minimal geochemical analysis for assessment of dustfall samples on a large scale is not well understood. Hence the major aim of this study has been to examine spatial-temporal variations in anthropogenic pollution from the monthly-based monitoring of magnetic properties of dustfall samples from contrasting environments.

Most areas of northern China are arid to semi-arid with sand and gravel (Gobi) deserts widespread (Zhu et al., 1980; Ye et al., 2000; Liu et al., 2004). Due to proximity of these deserts to the Beijing–Tianjin–Tangshan region, dust storms (frequent during the spring), commonly invade highly urbanised regions. In addition, rapid industrialization and increasing population density in these latter regions causes major in situ air pollution problems (Duan et al., 2006). In this study we contrast magnetic properties and metal concentrations in dustfall samples from these urban environments with rural Inner Mongolia. Samples (0.013–3.029 g with the mean mass of 0.541 g) were collected monthly during the interval April 2009–March 2010 to provide the first long-term study of magnetic properties of dustfall samples complemented by correlative investigation of heavy metals. Throughout the rock magnetic, chemical and statistical analysis of the particulates we have aimed to define regional and temporal variations in northern China and demonstrate the value of the interdisciplinary approach to environmental studies.

2. Sampling and methodology

2.1. Study area and sampling

The Hunshandake Sandy Land (HSL, Fig. 1) is 21,400 km^2 in area and belongs to the eastern desert belt of northern China (Zhu et al., 1980). Each year there are 50–110 windy days with wind velocities $\geq$5 m s^{-1} capable of moving sand (Yang et al., 2008). Since the HSL lies directly upwind of the Beijing and Tianjin metropolitan areas, dust is transported by strong winds through Inner Mongolia, Hebei Province, the Beijing–Tianjin–Tangshan area and ultimately to Korea and Japan (Cao et al., 2002). In Inner Mongolia, with the exception of a N–S road corridor crossing the HSL, there is no centralized residential area. People live mostly in separated

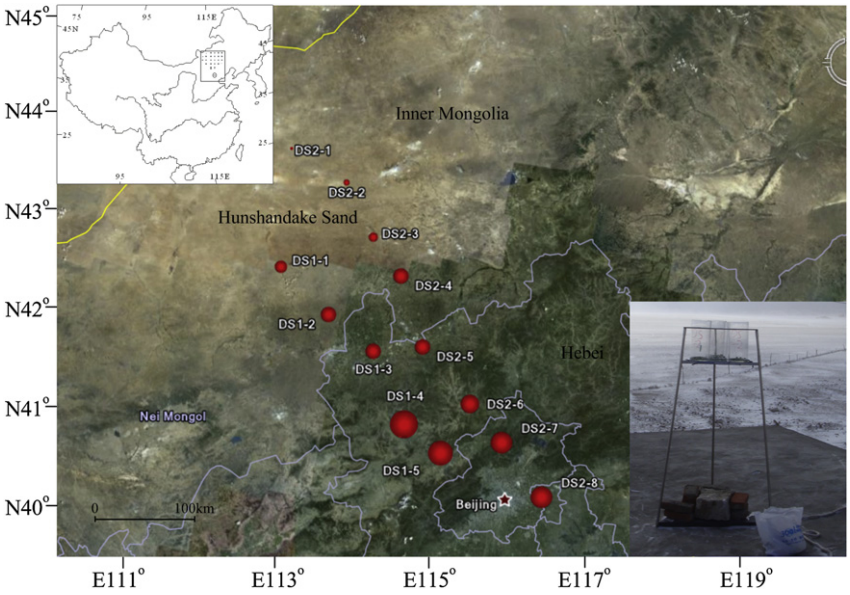

Fig. 1. Sketch map showing the sampling locations (red dots) and Hunshandake desert areas around Beijing. The sizes of the dot symbols define the mean magnetic susceptibility values. The inset picture illustrates the sampling device used for this study.

Author's personal copy

Table 1
Summary of magnetic parameters of atmospheric PM for the sample collection from Inner Mongolia, Hebei Province and Beijing.

Site			χ (10^{-8} m^3 kg^{-1})	SIRM (10^{-3} Am^2 kg^{-1})	ARM (10^{-6} Am^2 kg^{-1})	χ_{ARM} (10^{-8} m^3 kg^{-1})	S-ratio
IM	($n = 96$)	Range	5.71–185.24	1.49–128.40	7.66–392.73	19.24–986.53	0.73–0.99
		Mean ± SD	57.71 ± 39.12	14.44 ± 15.88	98.83 ± 69.43	248.27 ± 174.39	0.91 ± 0.05
HB	($n = 36$)	Range	54.74–1438.17	3.91–375.34	79.21–1819.45	198.99–4570.47	0.76–0.99
		Mean ± SD	370.91 ± 304.08	66.17 ± 75.20	321.95 ± 309.95	808.75 ± 778.59	0.93 ± 0.06
BJ	($n = 24$)	Range	96.39–366.59	6.40–316.92	36.93–1661.92	92.77–4174.75	0.88–0.98
		Mean ± SD	208.68 ± 75.62	64.32 ± 69.30	349.67 ± 353.63	878.38 ± 888.31	0.95 ± 0.02
Total	($n = 156$)	Range	5.71–1438.17	1.5–375.34	7.66–1819.45	19.24–4570.47	0.73–0.99
		Mean ± SD	166.24 ± 209.14	32.25 ± 47.57	194.89 ± 243.73	489.57 ± 612.25	0.92 ± 0.05

households and cover large areas for pasturing animals (Yang et al., 2007). In contrast, Hebei Province at the heart of one of two major industrial regions in China, has an industrial infrastructure incorporating coal, iron, textiles, oil and steel.

The present study employs magnetic measurements conducted on the contents of monthly containers collected from 13 monitoring stations. The selected sites are distributed across the HSL (Fig. 1) with six (DS1-1, 1-2, 2-1, 2-2, 2-3 and 2-4) in Inner Mongolia. Four (DS1-1, 2-1, 2-2, 2-3) are in countryside far from pollution sources and representative of the rural background. Another seven (DS1-3, 1-4, 1-5, 2-5, 2-6, 2-7 and 2-8) record contrasting examples of anthropogenic pollution through Hebei and Beijing: DS1-3, 2-5, 2-6, 2-7 are in suburban environment with little industrial activity, whilst DS1-4, 1-5 and 2-8 are representative of high-traffic industrial areas. A total of 156 dustfall samples were determined by the gravimetric method at monthly intervals from April 2009 to March 2010. The dust samples were collected in 15 × 30 cm cylindrical glass vessels with crystal balls on the base and these vessels were placed on a 1.5 m sampling frame to avoid small particles being removed by wind above the ground. Sites were located in open areas to avoid local aberrant dust sources influencing the samples (Fig. 1). Inner Mongolia has a low annual rainfall rate mostly as drizzle and effects of rain-out/rain splash can be ignored. The other sites had manual roofs used during rain or snow to prevent the loss of previously-collected particulate.

2.2. Laboratory methods

All samples were air-dried and sieved through a 1 mm mesh to remove obvious refuses and the dust was tightly packed into 10cc polyethylene cubes for magnetic measurements in the Paleomagnetism and Geochronology Laboratory at the Institute of Geology and Geophysics, Chinese Academy of Sciences. Magnetic susceptibilities were initially measured using a Kappabridge KLY-3 and Anhysteretic Remanent Magnetizations (ARM) were imparted in a peak alternating field (AF) of 80 mT with a superimposed direct current (DC) bias field of 0.05 mT parallel to the AF. Isothermal Remanent Magnetization (IRM) determinations were performed with a Model 670 IRM Pulse Magnetizer with a field of 1.0 T designated as saturation IRM (SIRM). Remanences were measured using a 2G-760 U-channel system.

Thermomagnetic curves monitoring change in magnetic susceptibility during heating–cooling cycles were measured by AGICO Kappabridge KLY-3 coupled to a CS-3 high-temperature furnace for continuous measurements to 700 °C in an argon atmosphere. Low-temperature magnetic characteristics were determined with a Quantum Designs superconducting quantum interference device (SQUID) model XP-5 Magnetic Properties Measurement System (MPMS XP-5, sensitivity is 5.0 × 10^{-10} Am^2). Samples were first cooled from 300 to 5 K in a 2.5 T field. After retention at 5 K in a 2.5 T field for 60 s the field was removed and thermal demagnetization conducted from 5 to 300 K. The Verwey transition temperature (T_V) is defined from the first derivative of the magnetization versus temperature curve at the minimum.

Hysteresis cycles and measurements of IRM acquisition and backfield demagnetization employed a Princeton Measurements Corporation (PMC) MicroMag 3900 vibrating-sample magneto-meter in fields up to 1 T. Measurements provide information on coercive force (B_c), remanent coercive force (B_{cr}), saturation remanent magnetization (M_{rs}) and saturation magnetization (M_s). Parameters B_c and B_{cr} depend on composition and grain size while, for a given composition, M_{rs} depends more on grain size than concentration. Ratios M_{rs}/M_s and B_{cr}/B_c provide information on magnetic grain size and domain state.

The method used for chemical analysis is described by Yang et al. (2009). A particulate mass concentration (~10 mg) is digested by a Microwave Accelerated Reaction System (MARS, CEM Corporation) and samples are dried at 150 °C, redissolved in 2% nitric acid and analyzed by inductively-coupled plasma-mass spectrometry (ICP-MS, 7500a, Agilent) in the State Key Laboratory of Atmospheric Boundary Layer Physics and Atmospheric Chemistry. Concentrations of 15 trace elements (Na, Mg, Al, K, Ca, V, Cr, Mn, Fe, Co, Ni, Cu, Zn, Ba and Zn) were determined. Principal Component Analysis (PCA) and Cluster Analysis (CA) were performed using commercial statistics software package SPSS version 18.0 for Windows (SPSS Inc.).

The Tomlinson pollution load index (*PLI*, Tomlinson et al., 1980), which is frequently used to assess heavy metal toxicities and gauge by how much sample contents exceed element concentrations

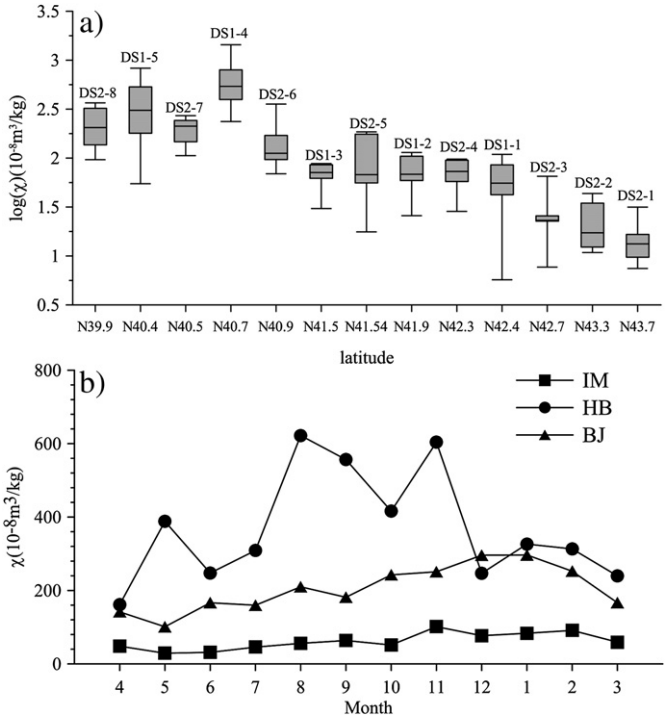

Fig. 2. Spatial and temporal variations in mean χ values for dustfall samples from Inner Mongolia, Hebei Province and Beijing. In Fig. 2b, IM: Inner Mongolia; HB: Hebei; BJ: Beijing. These regional abbreviations are used in the following figures.

Author's personal copy

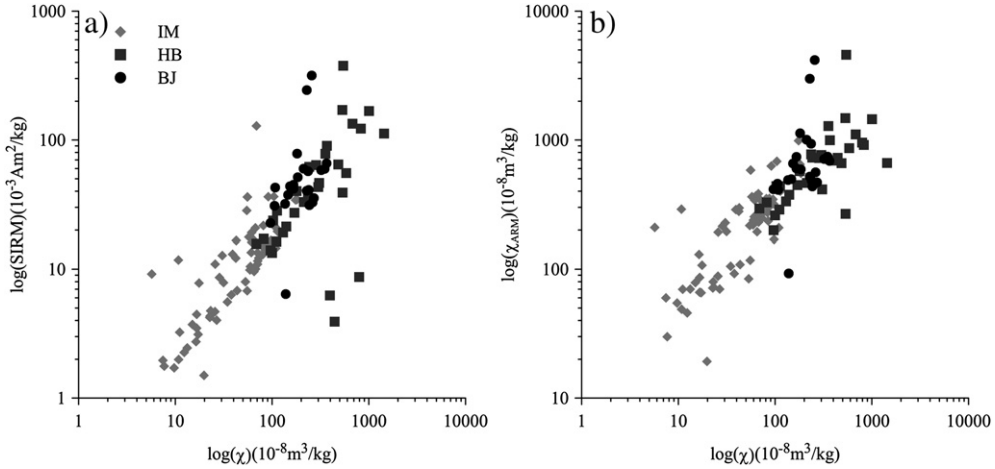

Fig. 3. Bi-plots of parameters plotted against each for data from IM, HB and BJ: (a) log (SIRM) versus log (χ); (b) log (χ_{ARM}) versus log (χ).

expected in the natural environments (e.g. Angulo, 1996), has been calculated from the element concentrations. The *PLI* is defined as the *n*-th root of the multiplication of concentration factors (CF_{HMn}), i.e. $PLI = (CF_{HM1}CF_{HM2}CF_{HM3}\ldots\ldots \times CF_{HMn})^{1/n}$, where CF_{HMn} is the ratio of the content of each heavy metal ($C_{HM,n}$) to its corresponding background value ($C_{background,n}$) or the lowest concentration value detected for each heavy metal ($C_{lowest,n}$). In this study background concentration values ($C_{background}$) in soils from Inner Mongolia, Hebei and Beijing were used to calculate the *PLI* index, respectively (Wei et al., 1990).

3. Results

3.1. Spatio-temporal variation of magnetic parameters

Magnetic parameters of dustfall for the 13 sites are summarized in Table 1. χ and SIRM values reveal distinctive spatial differences in magnetic concentrations (Table 1); site DS1-4 from Hebei shows highest values of each concentration parameter (see Fig. 1) whilst site DS2-1 in Inner Mongolia has the lowest values. We identify gradual increase in mean χ values from north to south (Figs. 1 and

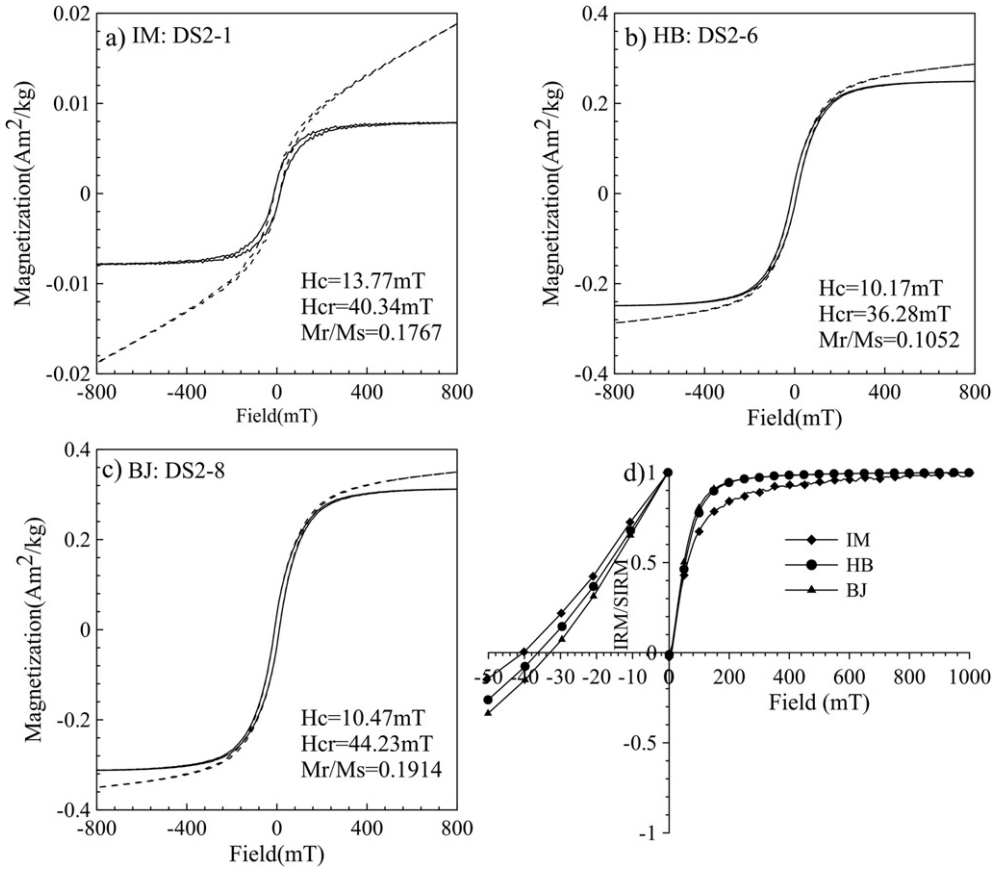

Fig. 4. Magnetic hysteresis loops (a–c), Isothermal remanent magnetization (IRM) acquisition and back-field demagnetization curves (d) for selected dustfall samples. In the magnetic hysteresis loops, the solid and dashed lines represent the corrected and original ones respectively.

Author's personal copy

2a). All χ values from DS2-1, DS2-2 and DS2-3 are less than 66×10^{-8} m^3 kg^{-1} and corresponding mean χ values less than 30×10^{-8} m^3 kg^{-1} in the order DS2-1 < DS2-2 < DS2-3 (Table 1, Figs. 1 and 2a); DS1-1, DS2-4, DS1-2, DS2-5 and DS1-3 show a wide range of χ values in the range $5.71–185.24 \times 10^{-8}$ m^3 kg^{-1}. All these latter stations except DS1-3 and DS2-5 are in Inner Mongolia with the latter two located close to the HSL and they can be reasonably grouped with Inner Mongolia. Sites in Hebei province typically have higher values whilst samples from the Beijing area (DS2-7, 2-8) show intermediate mean values (Table 1). We divide the 13 sampling sites into three categories on the basis of χ values to monitor spatial and temporal pollution variations (Inner Mongolia (IM): DS1-1, DS1-2, DS1-3, DS2-1, DS2-2, DS2-3, DS2-4 and DS2-5; Hebei Province (HB): DS1-4, DS1-5 and DS2-6; Beijing (BJ): DS2-7 and DS2-8).

Temporal variations in magnetic concentration are traced using χ in Fig. 2b. In Inner Mongolia samples have relatively constant χ values oscillating around 50×10^{-8} m^3 kg^{-1} independent of season. Samples from Hebei show high values in May, August and November 2009 and decrease in January. In Beijing χ values show a distinctly seasonal pattern being generally higher during the dry winter (Fig. 2b). The near-linear trend between the parameters (log (SIRM) vs log (χ), log (χ_{ARM}) vs log (χ)) in a binary diagram (Fig. 3) indicates that both are dominated by ferrimagnetic components in

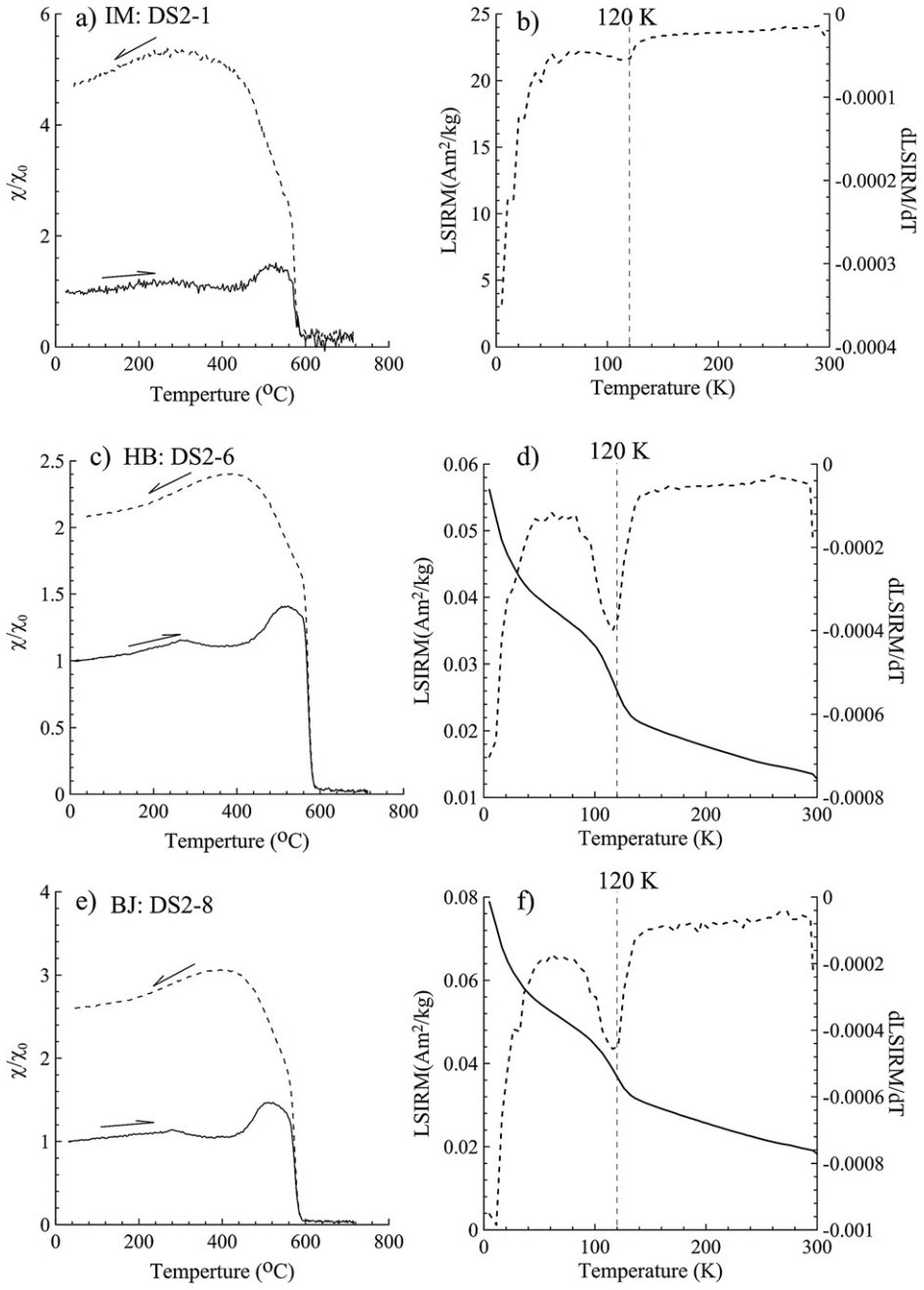

Fig. 5. Representative types of temperature-dependent magnetic susceptibility curves (a, c, e). Each curve is normalized with its corresponding magnetic susceptibility at room temperature χ_0. The solid and dotted lines denote heating and cooling runs, respectively. Low-temperature dependence of SIRM for the corresponding samples is also given (b, d, f). A measurement interval of 2 °C at a heating and cooling rate of about 9 °C per minute was used.

Author's personal copy

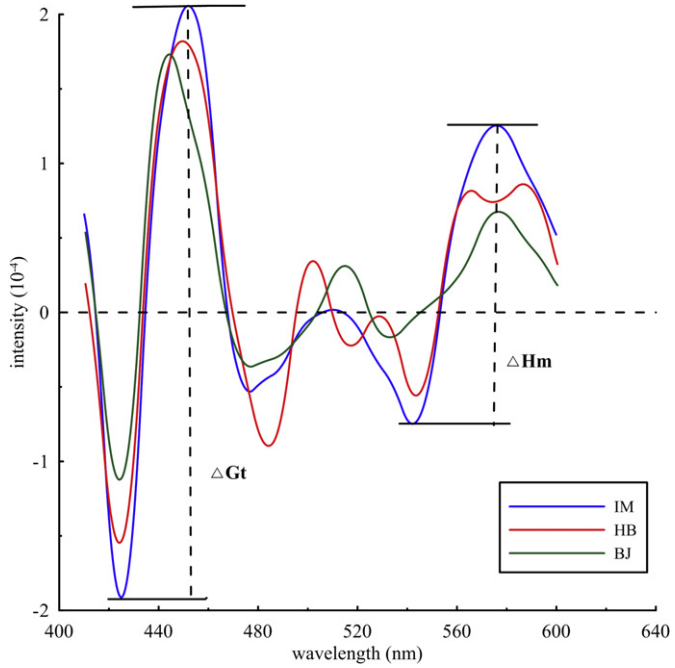

Fig. 6. The second derivative curves of the DRS for dustfall samples from the IM, HB and BJ regions. The dashed vertical lines mark the peak positions. See text for explanation.

the dustfall samples. Deviations from the linear trend suggest that the most significant differences between the sampling locations result from mineralogical contrasts.

3.2. Magnetic mineralogical properties

To identify the main magnetic phases in dustfall samples from the regions, three typical sites DS2-1 (IM), DS2-6 (HB) and DS2-8 (BJ) were subjected to more detail magnetic analysis. Narrow hysteresis loops closing below ~300 mT (Fig. 4) indicate dominant low coercivity ferromagnets, although closure values from Inner Mongolia are typically slightly higher than those from Hebei and Beijing (Fig. 4) and record relatively higher paramagnetic and/or high-coercivity contents here (Fig. 4a). IRM acquisition and back-field demagnetization curves (Fig. 4d) show rapid increase of IRM achieving near-saturation by a field of 300 mT; back-field demagnetization curves display softer behaviors with B_{cr} lower than 45 mT and reveal the coexistence of lower and higher-coercivity phases. Lower coercivity dominates behavior in areas HB and BJ whilst high-coercivity in samples from IM indicates that hematite and/or goethite contribute to the magnetic mineral content (Fig. 4d).

Magnetic minerals in dustfall samples can be confirmed by temperature-dependent susceptibility (χ-T) cycles when these are made in an argon atmosphere to prevent specimen oxidation (Fig. 5). Generally the curves display similar behaviors: on heating a very small peak is observed at 200–300 °C, followed by a wide peak near 500 °C, before approaching a Curie point (T_C) at ~585 °C defining the presence of magnetite (Dunlop and Özdemir, 1997). Increased susceptibility below 250 °C and peaks around 250–300 °C may indicate ultrafine particles reaching the single domain (SD) to superparamagnetic (SP) transition or alternatively a phase transition (Oches and Banerjee, 1996; Deng et al., 2004; Liu et al., 2005). Subsequent decrease up to ~580 °C identifies pure magnetite as the major contributor to χ and values are higher in the cooling curves at temperatures <580 °C. This effect is observed elsewhere in APM investigations (Muxworthy et al., 2002; Szönyi et al., 2008) and records magnetite formation by the heating (Zhang et al., 2010a, 2012a); it is obviously more important in Inner Mongolia than elsewhere and paramagnetic clays are a possible precursor (Fig. 5).

Further proof of magnetite in the dustfall samples is the clear Verwey transition at ~120 K (e.g. Fig. 5d and f) with the exception of the samples in Inner Mongolia (Fig. 5b). For stoichiometric MD magnetite this occurs at about 123 K whereas with increasing nonstoichiometry (maghemitization) the transition is gradually suppressed and shifted toward lower temperatures (Özdemir et al., 1993). The anomaly at 118 K on the LSIRM curve is much more pronounced for the Hebei and Beijing samples (Fig. 5d and f); it confirms that MD magnetite is developed as the dominant phase here and contrasts with the evidence from Inner Mongolia.

Since the much higher magnetic susceptibility of magnetite suppresses a signature of hematite and goethite in the χ-T determinations, we have conducted Diffuse Reflectance Spectra (DRS) investigation to clarify the presence of these minerals. DRS were recorded from 350 to 750 nm in 0.5 nm steps at a scan speed rate of 300 nm/min^{-1} using a Varian Cary 5000 spectrophotometer equipped with a $BaSO_4$-coated integrating sphere and using $BaSO_4$ as the white standard. The difference in ordinate between the

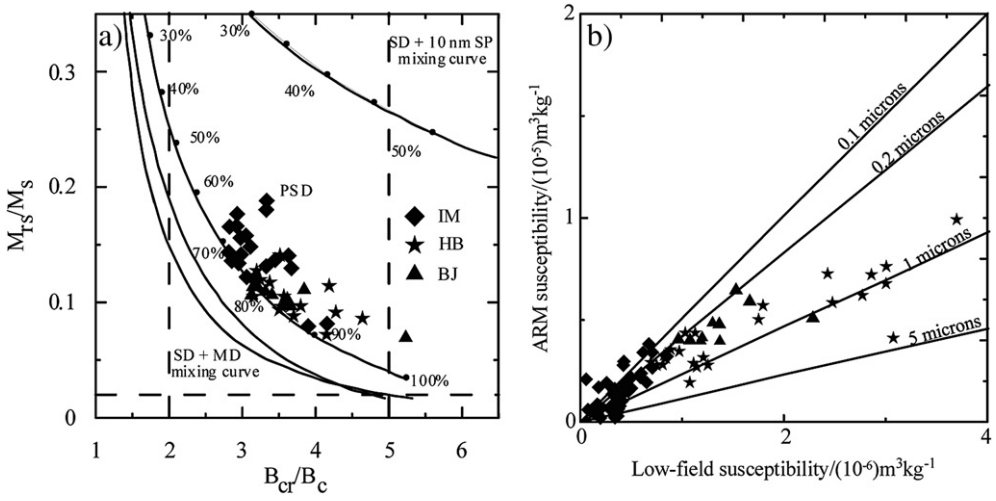

Fig. 7. Day plot of the ratios M_{rs}/M_s and B_{cr}/B_c and a King plot for the dustfall samples. The curve in (a) is the distribution of mixtures with single domain (SD) + multi-domain (MD) in pseudo-single domain (PSD) ranges after Dunlop (2002). The percentages are the MD particle percentages in the samples.

Author's personal copy

minimum and the next maximum at a longer wavelength can be used as a proxy for the true band amplitude and the intensities of the bands at ~425 nm and ~535 nm are proportional to the concentration of goethite and hematite, respectively (Scheinost et al., 1998). Fig. 6 compares the spectra in dustfall from the three regions and confirms the presence of significant amounts of hematite and/or goethite in the material.

In the Day plot (Fig. 7a) most samples are distributed over the pseudo-single-domain (PSD) range with the IM samples plotting closer to the SD field. The distribution of HB and BJ samples in the Day plot (Fig. 7a) shows that multidomain (MD) contributes 80–90% whilst it is less (60–80%) in the IM sample; hence magnetic grain size is generally coarser in the urban materials.

A higher slope in the King plot (χ_{ARM}/χ) indicates smaller magnetic grain-sizes provided that samples do not contain SP particles (King et al., 1982). SP particles do not contribute to the remanent magnetization (e.g. ARM and SIRM) but can significantly increase the value of χ. In Fig. 7b grain sizes are seen to be mostly smaller than 1 μm and the plot highlights two distinct observations. Firstly, χ for the Inner Mongolia dustfall is substantially smaller than for the urban sites reflecting the relatively lower magnetite concentrations (Fig. 7b). Secondly, the IM samples show higher slopes of χ_{ARM}/χ suggesting that the magnetite here is finer-grained, a point also confirmed by the results of the Day plot (Fig. 7a).

In summary, PSD- to MD magnetite is the dominant magnetic phase in the HB and BJ urban dustfall whereas the rural IM sample has higher concentration of finer grain sizes including a significant contribution from a high-coercivity phase.

3.3. Heavy metal concentrations

Heavy metal concentrations are listed in Table 2 and comparative concentrations of Fe, Co, Cr, Pb, Zn, Mn, Cu, V and Ni are shown in Fig. 8. The mean concentrations of Fe, Co, Pb, Zn, Cu, V and Ni are the highest in Hebei while the lowest are in Inner Mongolia with the exception of Co (Fig. 8 and Table 2). The lowest mean concentration of Co and highest mean concentration of Cr is found in Beijing. A pillar industry using silicomanganese near sampling site DS1-2 from Inner Mongolia results in the highest concentration of Mn here (Table 2, Fig. 8d). Table 2 also shows the values of the *PLI* in the three areas. According to the classification of Ding et al. (2005, see Table 2 footnote) the Inner Mongolia sites are defined as unpolluted whereas the Hebei and Beijing sites are characterized by moderate pollution.

3.4. Correlations of heavy metal concentrations and magnetic parameters

For this analysis two multivariate techniques, principal component analysis (PCA) and cluster analysis (CA), are applied. PCA identifies patterns and emphasizes similarities and differences in data (Shin et al., 2010). In combination these methods provide powerful tools for identifying sources and understanding distributions of trace metals in dustfall (e.g. Jalkanen and Manninen, 1996; Ragosta et al., 2001). PCA with varimax normalized rotation on the dataset of metals is performed for source identification and Table 3 lists the PC loadings with Eigen values >1 and accommodating >85% of total variance. In the event, the PC1 explaining most of the variance (34.48%) has maximum loadings for Mg, Ca, Fe, V, Cu and Co and is supported by the CA. The PC2 shows higher loadings for Ba, Zn, Pb and explains 20.24% of the total variance; the PC3 reveals maximum loadings for Al and Mn (16.03%). The PC4, which presents the high loadings for Cr and Ni, accounts for 15.1% of the total variance. Relationships between metals based on the first

Table 2
Statistics of the heavy metal content and PLI in the atmospheric PM samples for the sample collection from Inner Mongolia, Hebei Province and Beijing. The values are in mg kg^{-1} except for Fe where values are in g kg^{-1}.

		Fe (g kg^{-1})	V (mg kg^{-1})	Cr (mg kg^{-1})	Mn (mg kg^{-1})	Co (mg kg^{-1})	Ni (mg kg^{-1})	Cu (mg kg^{-1})	Zn (mg kg^{-1})	Pb (mg kg^{-1})	PLI
IM ($n = 16$)	Max	26.74	55.26	50.14	1538.42	17.56	50.84	43.93	234.3	95.11	1.78
	Min	3.97	9.86	9.01	78.01	0.29	3.39	4.55	20.33	17.77	0.29
	Mean ± SD	15.33 ± 8.26	35.32 ± 18.28	29.71 ± 5.96	537.98 ± 479.6	9.22 ± 5.04	18.41 ± 13.43	19.68 ± 12.66	97.01 ± 65.59	38.33 ± 27.15	0.89 ± 0.49
HB ($n = 6$)	Max	41.86	96.06	259.54	686.5	19.72	47.19	83.01	1852.84	474.73	2.2
	Min	25.87	52.8	56.37	474.51	11.27	25.81	41.14	201.67	69.46	1.2
	Mean ± SD	34.49 ± 5.99	78.23 ± 16.28	111.28 ± 77.21	587.82 ± 77.37	15.54 ± 3.09	31.68 ± 7.82	59.53 ± 15.40	550.38 ± 640.28	179.28 ± 149.21	1.50 ± 0.34
BJ ($n = 7$)	Max	26.21	61.32	447.95	716.65	9.24	80.28	70.78	414.03	125.21	1.45
	Min	16.24	37.69	35.17	352.75	3.74	17.01	27.48	226.93	67.16	0.82
	Mean ± SD	20.36 ± 3.41	43.70 ± 8.16	129.8 ± 157.97	452.4 ± 129.7	7.08 ± 2.26	30.82 ± 23.67	50.35 ± 15.89	305.63 ± 70.08	106.02 ± 20.54	1.06 ± 0.23

Footnote: degrees of pollution are defined as follows: $0 < PLI \leq 1$ unpolluted; $1 < PLI \leq 2$ moderately polluted; $2 < PLI \leq 3$ highly polluted; $3 < PLI \leq 4$ very highly polluted.

Author's personal copy

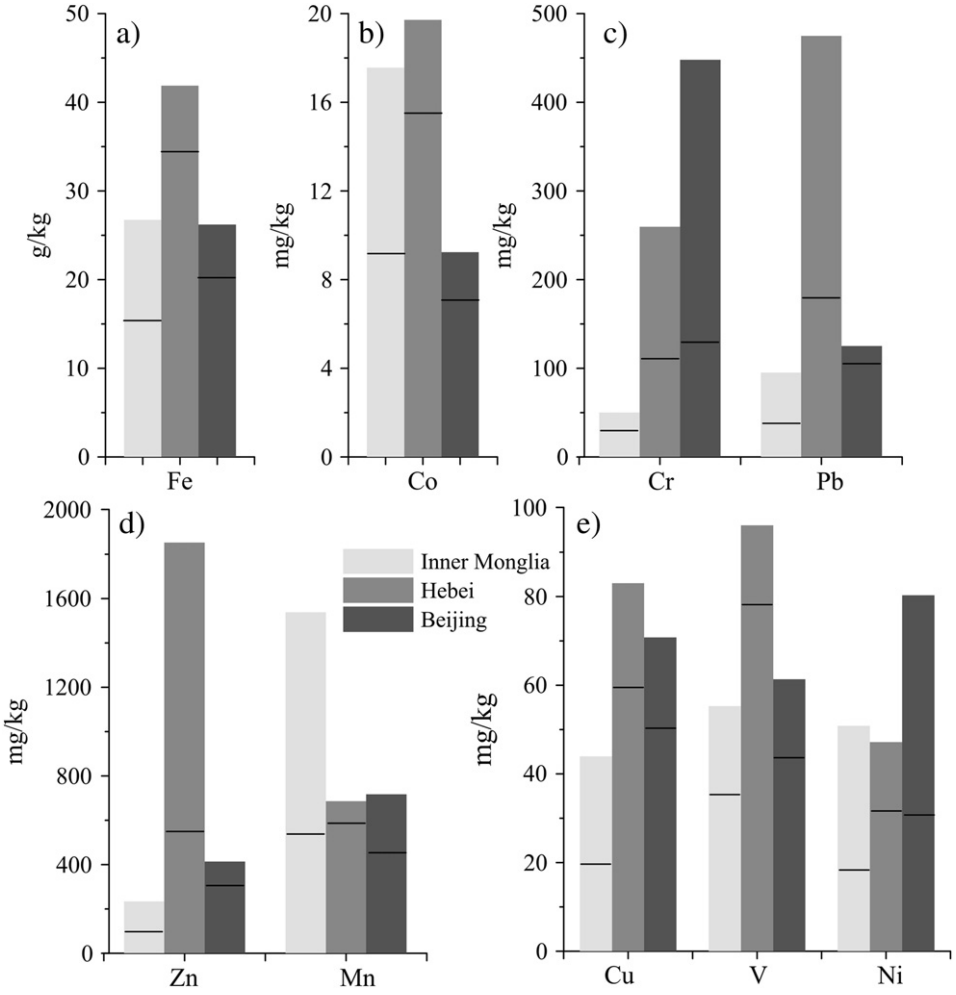

Fig. 8. Comparison of mean heavy metal concentrations of dustfall samples in the three regions (Inner Mongolia, Hebei and Beijing); the line in the box indicates the mean values.

three principle components of the dustfall are illustrated in 3D space in Fig. 9a.

CA was performed to further evaluate similarities of the concentration-dependent magnetic parameters and metal sources by applying the between-group linkage method. The corresponding dendrogram is shown in Fig. 9b and displays two main clusters: (i) V, Fe, χ, Mg, Ca, Cu, Co, SIRM, ARM, Zn, Pb, Ba; and (ii) Cr, Ni, Al, Mn, Na, K. Elements in cluster (i) join together at a relatively high level indicating that anthropogenic metals such as V, Fe, Mg, Ca, Cu, Co, Zn, Pb and Ba are mainly associated with χ, SIRM and ARM. In contrast Cr and Ni in cluster (ii) show a far greater distance and Al, Mn, Na and K show a further distance.

Table 3
Rotated Component Matrix[a] for data of PM samples (PCA loadings >0.5 are shown in bold).

	Components			
	1	2	3	4
Na	−0.047	**0.665**	−0.206	0.075
Mg	**0.903**	0.143	0.029	0.209
Al	−0.170	−0.050	**0.945**	−0.004
K	−0.893	−0.087	0.239	−0.208
Ca	**0.857**	0.036	0.105	0.283
V	**0.801**	0.270	0.397	0.146
Cr	0.224	0.064	−0.039	**0.915**
Mn	0.279	−0.025	**0.770**	0.313
Fe	**0.819**	0.265	0.418	0.185
Co	**0.519**	0.237	**0.540**	−0.154
Ni	0.356	0.001	0.358	**0.850**
Cu	**0.739**	0.148	−0.035	**0.585**
Zn	0.376	**0.899**	0.041	0.063
Ba	0.030	**0.940**	0.209	−0.059
Pb	**0.516**	**0.802**	0.084	0.078
% of variance	34.477	20.241	16.026	15.102
Cumulative %	34.477	54.717	70.744	85.846

Extraction Method: Principal Component Analysis, Rotation Method: Varimax with Kaiser Normalization.
[a] Rotation converged in 6 iterations.

Pearson correlation coefficients (P) between metal concentrations and magnetic parameters are listed in Table 4. χ and SIRM have significant positive correlations with Fe, Zn, Pb, V and Mg and show negative correlation with K and Al. Since P coefficients between χ and metals are highest amongst the magnetic parameters, we select χ for quantifying the relationship between magnetic parameters and metals. The scatter plots of χ versus Cu, Pb, Fe, Zn, Cr and Al are given in Fig. 10 which includes the coefficient of determination R^2 values. All metals except Al ($R^2 = 0.012$) show good correlation with χ i.e., Cu ($R^2 = 0.752$), Pb ($R^2 = 0.731$), Fe ($R^2 = 0.713$), Zn ($R^2 = 0.684$), Cr ($R^2 = 0.511$).

4. Discussions

4.1. Sources of magnetic minerals and heavy metals

IRM and DRS analysis of dustfall from rural regions of Inner Mongolia in northern China identifies high-coercivity magnetic minerals such as hematite and goethite complementing SD and SP

Author's personal copy

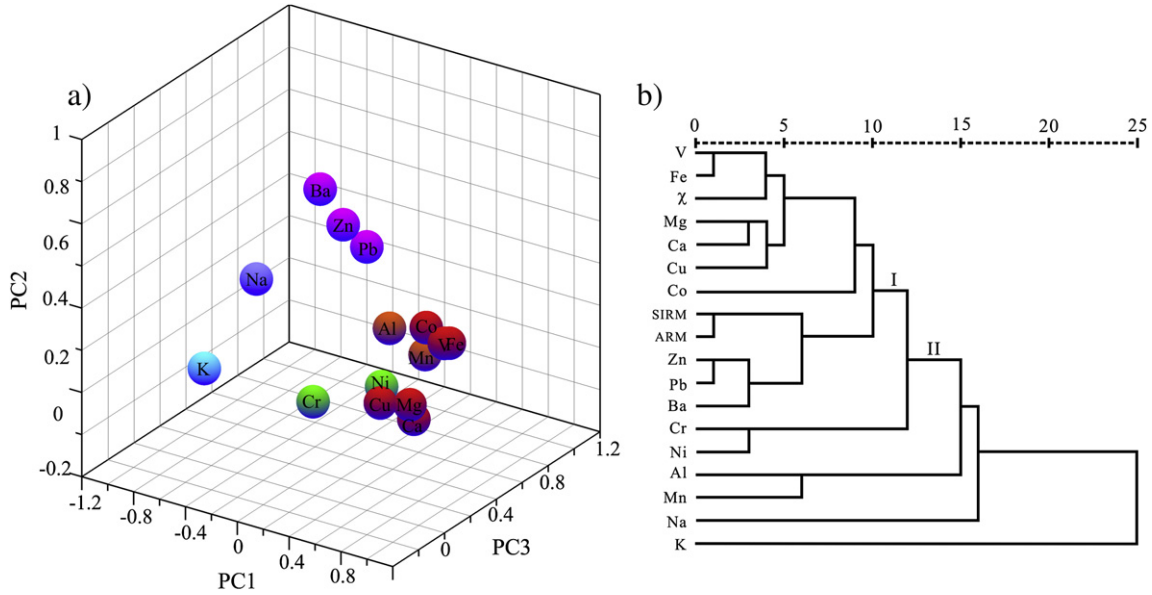

Fig. 9. (a) PCA results of dustfall samples in three-dimensional space: plots of loading of the first three principal components (different colour refer to different cluster-groups); (b) Dendrogram results of all samples from the Between-group linkage method of hierarchical cluster analysis for 15 elements and 3 magnetic parameters.

magnetite particles. Residual amounts of these minerals remain in samples from the urban regions although coarse grained magnetite dominates magnetic content in these latter environments (Figs. 4–7). The multivariate statistical analysis (Fig. 9 and Table 3) shows metal contents separating into four groups. Group I including V, Fe, Mg, Ca, Cu and Co reveals significant correlations with χ, while Zn, Pb, Ba in the Group II show significant correlations with SIRM and ARM, indicating that these heavy metals come from different sources (Fig. 9b); group III includes Cr and Ni and shows less correlation with χ, SIRM and ARM. All these metals are likely to originate predominantly from anthropogenic activities. The first transition group elements (V, Cr, Fe, Co, Ni, Cu and Zn) are rich in the magnetic spinel fraction of fly-ash (Hulett et al., 1980), and Mg and Ca are mostly enriched in construction materials (Shu et al., 2001). Cr, Cu and Zn are released by metallurgical industries whilst traffic pollution involves a wide range of trace element emissions including Fe, Ba, Pb, Cu and Zn (Pacyna, 1986). Each of these metals can become dustfall from emissions of slag, dust and exhaust gases in urban environments. In contrast, Al, Mn, Na and K (Group IV) including lighter metals show zero or negative correlation with magnetic parameters (Table 4 and Fig. 9), whilst s-block elements such as Na and K and p-block elements such as Al and Mn are enriched in soil and other pedogenic sources (Shu et al., 2001); these metals are likely to be sourced in wind-blown natural particles.

Table 4
Pearson's correlations matrix for the heavy metals concentrations and magnetic parameters ($n = 29$).

	χ	SIRM	ARM	S-ratio
Na	0.245	0.055	−0.020	−0.305
Mg	0.778**	0.559**	0.499**	0.539**
Al	−0.152	−0.191	−0.137	0.255
K	−0.689**	−0.577**	−0.533**	−0.506**
Ca	0.607**	0.393*	0.338	0.494**
V	0.799**	0.495**	0.433*	0.586**
Cr	0.210	0.058	0.032	0.364
Mn	0.153	0.080	0.107	0.423*
Fe	0.803**	0.492**	0.428*	0.600**
Co	0.450*	0.184	0.111	0.481**
Ni	0.276	0.107	0.100	0.482**
Cu	0.653**	0.308	0.241	0.413*
Zn	0.647**	0.720**	0.643**	0.078
Ba	0.419*	0.591**	0.540**	−0.049
Pb	0.676**	0.739**	0.665**	0.161
PLI	0.639**	0.454*	0.406*	0.535**

*Correlation is significant at the 0.05 level (2-tailed).
**Correlation is significant at the 0.01 level (2-tailed).

Various APM pollution sources are documented from China by previous studies (Zhang et al., 1998; Wang et al., 2002, 2005; Duan et al., 2004) with combustion of coal recognized as the principal source (Millman et al., 2008). The vast industrial network in the country relies on coal for ~70–75% of energy needs compared with 14%, 22%, and 53% for Japan, the USA and India, respectively (Zhang et al., 2002); 70% of Chinese households burn coal or biomass (Jin et al., 2005). In addition the rapidly-increasing population of motor vehicles is an expanding contributor to air pollution near transport arteries; almost nonexistent before 1978, car numbers had reached more than 29 million by late 2006 (China National Statistics Bureau, 2006). Traffic is a major source of toxic elements such as Pb and Zn (Chillrud et al., 1999) and remains high in Chinese urban dusts even after abatement of leaded fuels (Millman et al., 2008). Thus elevated concentrations of Fe, Co, Pb, Zn, Cu and V in Hebei province (Table 2 and Fig. 8) are attributable to collective emissions of industrial plant and vehicles.

4.2. Implications for magnetic mapping of urban atmospheric environment

Spatial variation of χ as characterized by scatter-plot and box-plot distinctions (Figs. 1 and 2) identifies highest magnetization in Hebei province evidently due to anthropogenic factors, whilst in rural Inner Mongolia there is no significant industry, most people ride horses although motorcycles are used by the wealthier, and χ of the dustfall is low. It is relatively higher in the vicinity of Beijing where pollutant emissions tend to be trapped by the topography.

To express temporal variations in magnetic parameters (e.g. χ in Fig. 2b) PCA analysis is applied in a regional context. Following PCA the information is mainly concentrated on the first components

Author's personal copy

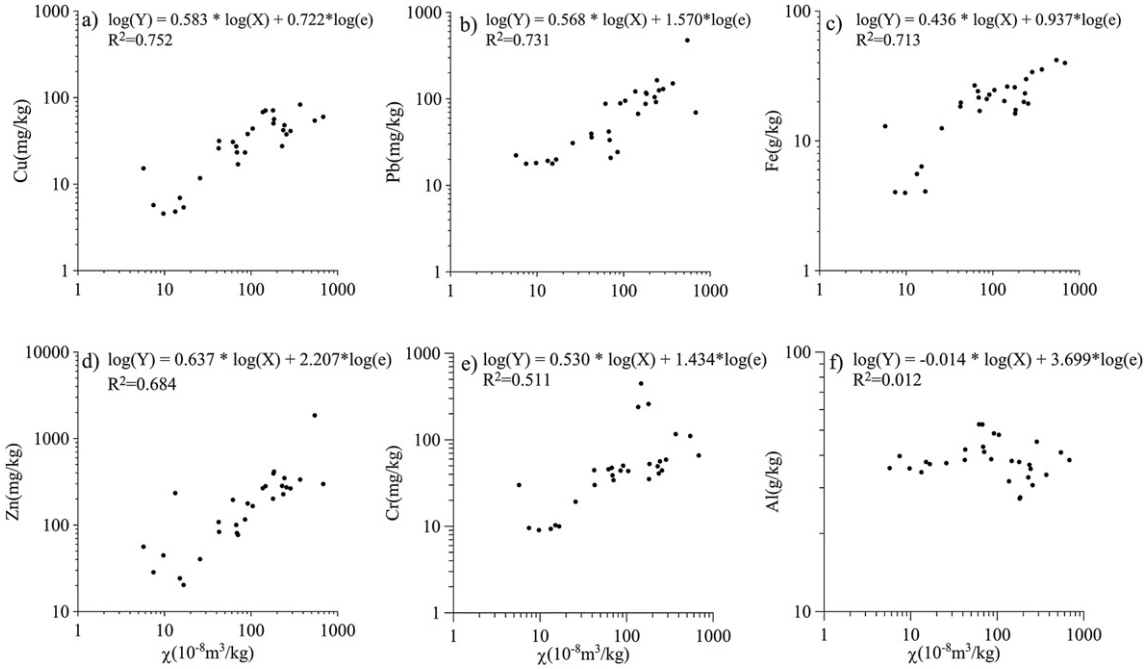

Fig. 10. The relationship between χ and (a) Cu, (b) Pb, (c) Fe, (d) Zn, (e) Cr and (f) Al for all samples. Equations and coefficients of determination between χ and the metals contents are listed on the figures.

(PC1) and the analysis provides the most meaningful variables to highlight sources of variation (Singh et al., 2004, 2005). Table 5 lists the PC1 loadings for the three areas and shows that Mn explains most of the variance in Inner Mongolia. The PC1 has maximum loadings for Zn, Ba, Pb in Hebei, while the PC1 in Beijing reveals maximum loadings for Cr, Mn and Ni. Mn shows no correlation with magnetic parameters (Table 4) indicating that magnetic materials in dustfall from Inner Mongolia come from other sources. Zn, Ba, Pb have significant positive correlations with χ and SIRM (Table 4 and Fig. 10). These three metals are released by industrial activities and traffic so the obvious increment during August to November in Hebei is possibly related to increased industrial emissions and contributions from mobile sources; thus Cr and Ni are enriched in the magnetic spinel fraction from fly-ash produced by industrial and domestic coal burning, with the latter explaining the higher influx of anthropogenic particulates from heating systems in the Beijing area during the winter (Fig. 2b).

Table 5
Rotated Component Matrix[a] for data of PM samples (PCA loadings >0.95 are shown in bold).

	Location		
	Inner Mongolia	Hebei	Beijing
Na	−0.006	0.738	−0.060
Mg	0.870	0.003	−0.456
Al	0.849	0.182	0.612
K	−0.446	−0.085	0.658
Ca	0.918	−0.039	0.463
V	0.771	0.439	0.862
Cr	0.809	−0.030	**0.981**
Mn	**0.957**	0.464	**0.964**
Fe	0.864	0.502	0.733
Co	0.371	0.705	0.231
Ni	0.923	−0.042	**0.970**
Cu	0.903	−0.211	0.734
Zn	0.756	**0.980**	−0.211
Ba	0.081	**0.970**	0.192
Pb	0.937	**0.977**	−0.735

Extraction Method: Principal Component Analysis, Rotation Method: Varimax with Kaiser Normalization.
[a] Rotation converged in 6 iterations.

In the King plot (Fig. 7b) particle sizes for our samples are mostly smaller than 1 μm. These ultrafine particles can pass through to the distal respiratory system to initiate cardiopulmonary disease; populations exposed to large fractions of this material in regions of high APM concentration can anticipate irreversible damage to their respiratory systems. Thus tracing the deposition of APM is important because of the threat to human health (Blundell et al., 2009). Among the range of magnetic concentration parameters, the correlation coefficients between χ and metals proves to be the highest (Table 4) and is therefore the optimum proxy parameter for detection of metals in dustfall samples.

The Tomlinson *PLI* including Fe, V, Mg, Ca, Cu, Co, Zn, Pb and Ba has been calculated for all samples to evaluate contamination degree from heavy metal input; it is termed PLI_{anthro} (Zhang et al., 2011). The strength of correlation with log (χ) declines for *PLI* for all metals compared with PLI_{anthro}. Scatter plots of log (χ) versus *PLI* and PLI_{anthro} are shown in Fig. 11; the coefficient of determination ($R^2 = 0.714$) with PLI_{anthro} is higher than with *PLI* ($R^2 = 0.574$) based on a linear equation (Fig. 11). This reinforces the finding that the magnetic concentration parameter log (χ) is proportional to the concentration of the sum of metals Fe, V, Mg, Ca, Cu, Co, Zn, Pb and Ba and is therefore a proxy measure of pollution sources in dustfall samples.

Spatial distributions of log (χ) and PLI_{anthro} show high values in the urban HB and BJ areas and low values in rural IM with an increasing trend from north to south (Figs. 2a and 12a). Samples from IM show relatively constant PLI_{anthro} values independent of seasonal change; on entering the Hebei and Beijing areas PLI_{anthro} values increase gradually from 1 to 2; this applies especially to samples from BJ which show a distinctive seasonal pattern with generally higher values in the dry winter compared with the rainy summer (Table 2, Fig. 12b).

Author's personal copy

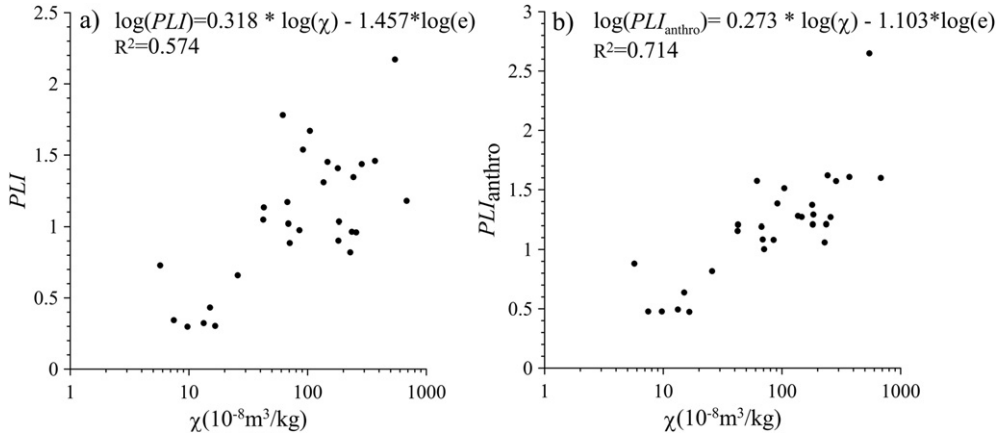

Fig. 11. The relationship between (a) χ and *PLI*, (b) χ and PLI_{anthro} for all dustfall samples. Equations and coefficient of determination (R^2) between ln (χ) and *PLI*, PLI_{anthro} are listed on the Figure. PLI_{anthro} refers to the Tomlinson *PLI* of Fe, V, Mg, Ca, Cu, Co, Zn, Pb, and Ba in atmospheric PM samples originating from anthropogenic activities.

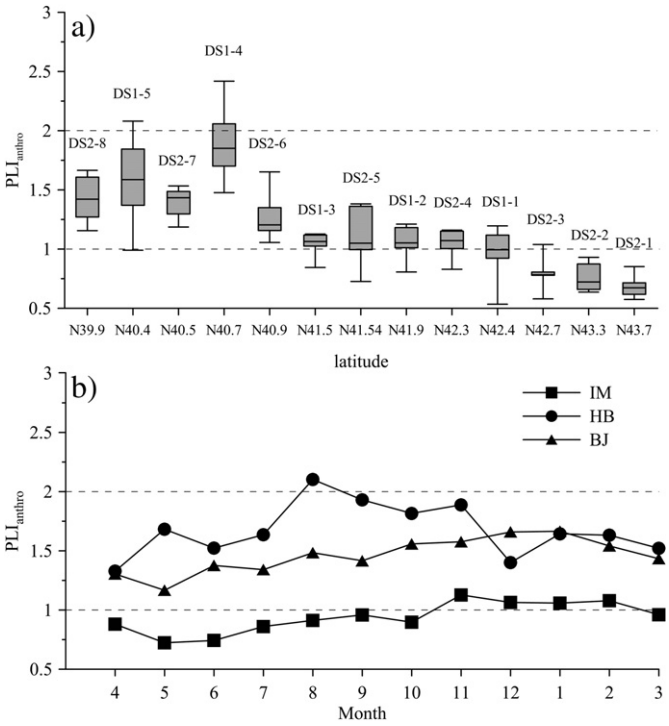

Fig. 12. Spatial distribution of PLI_{anthro} (*PLI* of anthropogenic heavy metals). $PLI_{anthro} \leq 1$: unpolluted; $1 < PLI_{anthro} \leq 2$: moderately polluted; $2 < PLI_{anthro} \leq 3$: highly polluted; $3 < PLI_{anthro} \leq 4$: very highly polluted (Ding et al., 2005).

5. Conclusions

Dustfall samples in rural Inner Mongolia incorporates fine SD magnetite with a significant contribution of a high coercivity ferromagnet (hematite, goethite) and paramagnetic minerals presumably clays.

This fraction is anticipated as a finer grained size residual fraction downwind in dustfall samples from Hebei and Beijing and recognized from IRM and DRS study. However, due to its high magnetic susceptibility the thermal signature here is dominated by larger grain sizes of PSD and MD magnetite of anthropogenic origin from industrial and traffic emissions. In Beijing the variations are seasonal due to the contribution of domestic coal burning.

Significant correlations between concentrations of important heavy metals (e.g., V, Fe, Zn, Cu, Co and Pb) and log (χ) demonstrate that magnetic parameters provide a simple, rapid and non-destructive proxy for determining anthropogenic contributions to dustfall samples. Specifically the Tomlinson pollution load index PLI_{anthro} (Fe, V, Mg, Ca, Cu, Co, Zn, Pb and Ba) provides a quantitative assessment of heavy metal pollution.

Acknowledgements

We are particularly grateful to Eduard Petrovský and an anonymous reviewer for valuable comments that permitted substantial improvements to the initial manuscript. DRS experiment assistance from Zhaoxia Jiang is highly appreciated. This study was supported by the National Natural Science Foundation of China (Grants 41104042, 40804014 and 20677059).

References

Angulo, E., 1996. The Tomlinson Pollution Load Index applied to heavy metal, 'Mussel-Watch' data: a useful index to assess coastal pollution. Science of the Total Environment 187, 19–56.

Beckwith, P.R., Ellis, J.B., Revitt, D.M., Oldfield, F., 1986. Heavy-metal and magnetic relationships for urban source sediments. Physics of the Earth and Planetary Interiors 42, 67–75.

Bell, J.N.B., Treshow, M., 2002. Air Pollution and Plant Life. John Wiley, Near York, pp. 187–199.

Blundell, A., Hannam, J.A., Dearing, J.A., Boyle, J.F., 2009. Detecting atmospheric pollution in surface soils using magnetic measurements: a reappraisal using an England and Wales database. Environmental Pollution 157, 2878–2890.

Cao, L., Tian, W.Z., Ni, B.F., Zhang, Y.M., Wang, P.S., 2002. Preliminary study of airborne particulate matter in a Beijing sampling station by instrumental neutron activation analysis. Atmospheric Environment 36, 1951–1956.

Chillrud, S.N., Bopp, R.F., Simpson, H.J., Ross, J.M., Shuster, E.L., Chaky, D.A., Walsh, D.C., Choy, C.C., Tolley, L.R., Yarme, A., 1999. Twentieth century atmospheric metal fluxes into central Park Lake, New York City. Environmental Science Technology 33, 657–662.

China National Statistics Bureau, 2006. Annual Report of Statistics on National Economic and Social Development (in Chinese). Available at: www.stats.gov.cn.

Choi, J.C., Lee, M., Chun, Y., Kim, J., Oh, S., 2001. Chemical composition and source signature of spring aerosol in Seoul, Korea. Journal of Geophysical Research 106, 18067–18074.

Choi, H., Zhang, Y.H., Kim, K.H., 2008. Sudden high concentration of TSP affected by atmospheric boundary layer in Seoul metropolitan area during duststorm period. Environment International 34, 635–647.

Dallarosa, J., Calesso Teixeira, E., Meira, L., Wiegand, F., 2008. Study of the chemical elements and polycyclic aromatic hydrocarbons in atmospheric particles of PM10 and PM2.5 in the urban and rural areas of South Brazil. Atmospheric Research 89, 76–92.

de Miguel, E., Llamas, J.F., Chacón, E., Berg, T., Larssen, S., Røyset, O., Vadset, M., 1997. Origin and patterns of distribution of trace elements in street dust: unleaded petrol and urban lead. Atmospheric Environment 31, 2733–2740.

Deng, C.L., Zhu, R.X., Verosub, K.L., Singer, M.J., Vidic, N.J., 2004. Mineral magnetic properties of loess/paleosol couplets of the central loess plateau of China over the last 1.2 Myr. Journal of Geophysical Research 109, B01103.

Author's personal copy

Ding, X.G., Ye, S.Y., Gao, Z.J., 2005. Methods of heavy metal pollution evaluation for offshore sediments. Marine Geology Letters 21, 31–36 (in Chinese).
Duan, F.K., Liu, X.D., Yu, T., Cachier, H., 2004. Identification and estimate of biomass burning contribution to the urban aerosol organic carbon concentrations in Beijing. Atmospheric Environment 38, 1275–1282.
Duan, F.K., He, K.B., Ma, Y.L., Yang, F.M., Yu, X.C., Cadle, S.H., Chan, T., Mulawa, P.A., 2006. Concentration and chemical characteristics of PM2.5 in Beijing, China: 2001–2002. The Science of the Total Environment 355, 264–275.
Dunlop, D.J., Özdemir, Ö., 1997. Rock Magnetism; Fundamentals and Frontiers. Cambridge University Press, Cambridge.
Dunlop, D.J., 2002. Theory and application of the Day plot (M_{rs}/M_s versus H_{cr}/H_c) 1. Theoretical curves and tests using titanomagnetite data. Journal of Geophysical Research 107. http://dx.doi.org/10.1029/2001JB000486.
Fang, G.C., Chang, C.N., Wu, Y.S., Lu, S.C., Fu Pi-Cheng, P., Chang, S.C., Cheng, C.D., Yuen, W.H., 2002. Concentration of atmospheric particulates during a dust storm period in central Taiwan, Taichung. Science of the Total Environment 287, 141–145.
Farmer, A., 1997. Managing Environmental Pollution. Routledge, London.
Halsall, C.J., Maher, B.A., Karloukovski, V.V., Shah, P., Watkins, S.J., 2008. A novel approach to investigating indoor/outdoor pollution links: combined magnetic and PAH measurements. Atmospheric Environment 42, 8902–8909.
Hulett, L.D., Weinberger, A.J., Northcutt, K.J., Ferguson, M., 1980. Chemcial-species in fly-ash from coal-burning power-plants. Science 210, 1356–1358.
Hunt, A., Jones, J., Oldfield, F., 1984. Magnetic measurements and heavy metals in atmospheric particulates of anthropogenic origin. Science of the Total Environment 33, 129–139.
Jalkanen, L., Manninen, P., 1996. Multivariate data analysis of aerosols collected on the Gulf of Finland. Environmetrics 7, 27–38.
Jin, Y., Zhou, Z., He, G., Wei, H., Liu, J., Liu, F., Tang, N., Ying, B., Liu, Y., Hu, G., Wang, H., Balakrishnan, K., Watson, K., Baris, E., Ezzati, M., 2005. Geographical, spatial, and temporal distributions of multiple indoor air pollutants in four Chinese provinces. Environmental Science Technology 39, 9431–9439.
Kim, W., Doh, S.J., Park, Y.H., Yun, S.T., 2007. Two-year magnetic monitoring in conjunction with geochemical and electron microscopic data of roadside dust in Seoul, Korea. Atmospheric Environment 41, 7627–7641.
Kim, W., Doh, S.J., Yu, Y., Lee, M., 2008. Role of Chinese wind-blown dust in enhancing environmental pollution in Metropolitan Seoul. Environmental Pollution 153, 333–341.
King, J., Banerjee, S.K., Marvin, J., Özdemir, Ö., 1982. A comparison of different magnetic methods for determining the relative grain-size of magnetite in natural materials-some results from lake sediments. Earth and Planetary Science Letters 59, 404–419.
Linton, R.W., Natusch, D.F.S., Solomon, R.L., Evans, C.A., 1980. Physicochemical characterization of lead in urban dusts. A microanalytical approach to lead tracing. Environmental Science and Technology 14, 159–164.
Liu, X.D., Yin, Z.Y., Zhang, X.Y., Yang, X.C., 2004. Analyses of the spring dust storm frequency of northern China in relation to antecedent and concurrent wind, precipitation, vegetation, and soil moisture conditions. Journal of Geophysical Research 109. http://dx.doi.org/10.1029/2004JD004615.
Liu, Q.S., Deng, C.L., Yu, Y.J., Torrent, J., Jackson, M.J., Banerjee, S.K., Zhu, R.X., 2005. Temperature dependence of magnetic susceptibility in an argon environment: implications for pedogenesis of Chinese loess/palaeosols. Geophysical Journal International 161, 102–112.
Maher, B.A., Moore, C., Matzka, J., 2008. Spatial variation in vehicle-derived metal pollution identified by magnetic and elemental analysis of roadside tree leaves. Atmospheric Environment 42, 364–373.
McIntosh, G., Gomez-Paccard, M., Osete, M.L., 2007. The magnetic properties of particles deposited on Platanus x hispanica leaves in Madrid, Spain, and their temporal and spatial variations. Science of the Total Environment 382, 135–146.
Millman, A., Tang, D., Perera, F.P., 2008. Air pollution threatens the health of children in China. Pediatrics 122, 620–628.
Morris, W.A., Versteeg, J.K., Bryant, D.W., Legzdins, A.E., McCarry, B.E., Marvin, C.H., 1995. Preliminary comparisons between mutagenicity and magnetic susceptibility of respirable airborne particulate. Atmospheric Environment 29, 3441–3450.
Muxworthy, A.R., Schmidbauer, E., Petersen, N., 2002. Magnetic properties and Mössbauer spectra of urban atmospheric particulate matter: a case study from Munich, Germany. Geophysical Journal International 150, 558–570.
Oches, E., Banerjee, S., 1996. Rock-magnetic proxies of climate change from loess -paleosol sediments of the Czech Republic. Studia Geophysical Et Geodaetica 40, 287–300.
Othmar, P., 1996. The many facets of aerosol science. Journal of Aerosol Science 27 (Suppl. 1), S1–S6.
Özdemir, Ö., Dunlop, D.J., Moskowitz, B.M., 1993. The effect of oxidation on the Verwey transition in magnetite. Geophysical Research Letters 20, 1671–1674.
Pacyna, M., 1986. Emission factors of atmospheric elements, and atmospheric trace elements from natural and authropogenic sources. In: Nriagu, J.O., Davidson, C.I. (Eds.), Toxic Metals in the Atmosphere. John Wiley, New York.
Petrovský, E., Ellwood, B.B., 1999. Magnetic monitoring of air-, land-, and water-pollution. In: Maher, B.A., Thompson, R. (Eds.), Quaternary Climates, Environments and Magnetism. Cambridge University Press, Cambridge.
Qiao, Q.Q., Zhang, C.X., Huang, B.C., Piper, J.D.A., 2011. Evaluating the environmental quality impact of the 2008 Beijing Olympic Games: magnetic monitoring of street dust in Beijing Olympic Park. Geophysical Journal International 187, 1222–1236.
Ragosta, M., Caggiano, R., D'Emilio, M., Macchiato, M., 2001. Multivariate analysis for investigating profile sources of atmospheric heavy metals emissions. Journal of Applied Statistical Sciences 10, 251–263.
Sagnotti, L., Taddeucci, J., Winkler, A., Cavallo, A., 2009. Compositional, morphological, and hysteresis characterization of magnetic airborne particulate matter in Rome, Italy. Geochemistry Geophysics Geosystems 10. http://dx.doi.org/10.1029/2009GC002563.
Scheinost, A.C., Chavernas, A., Barró, V., Torrent, J., 1998. Use and limitations of the second-derivative diffuse reflectance spectroscopy in the visible to near-infrared range to identify and quantify Fe oxide minerals in soils. Clays and Clay Minerals 46, 528–536.
Shin, E.–C., Craft, B.D., Pegg, R.B., Phillips, R.D., Eitenmiller, R.R., 2010. Chemometric approach to fatty acid profiles in runner-type peanut cultivars by principal component analysis (PCA). Food Chemistry 119 (3), 1262–1270.
Shu, J., Dearing, J.A., Morse, A.P., Yu, L., Yuan, N., 2001. Determining the sources of atmospheric particles in Shanghai, China, from magnetic and geochemical properties. Atmospheric Environment 35, 2615–2625.
Singh, K.P., Malik, A., Mohan, D., Sinha, S., 2004. Multivariate statistical techniques for the evaluation of spatial and temporal variations in water quality of Gomti River (India) – a case study. Water Research 38 (18), 3980–3992.
Singh, K.P., Malik, A., Sinha, S., 2005. Water quality assessment and apportionment of pollution sources of Gomi River (India) using multivariate statistical techniques – a case study. Analytica Chimica Acta 538 (1–2), 355–374.
Szönyi, M., Sagnotti, L., Hirt, A.M., 2008. A refined biomonitoring study of airborne particulate matter pollution in Rome, with magnetic measurements on Quercus Ilex tree leaves. Geophysical Journal International 173, 127–141.
Tomlinson, D.L., Wilson, J.G., Harris, C.R., Jeffrey, D.W., 1980. Problems in the assessment of heavy-metal levels in estuaries and the formation of a pollution index. Helgoländer Meeresunters 33, 566–575.
Verosub, K.L., Roberts, A.P., 1995. Environmental magnetism-past, present, and future. Journal of Geophysical Research 100, 2175–2192.
Wang, W., Yue, X., Liu, H.J., Pan, Z., Tang, D.G., Wang, Y., Du, Y.G., Su, H.M., Qian, F., Ban, B.Y.H., 2002. Study on pollution characteristics of aerosols during sand dust storm weather in Beijing. Acta Scientiae Circumstantiae 22, 494–498 (in Chinese with abstract in English).
Wang, Y., Zhuang, G.S., Tang, A.H., Yuan, H., Sun, Y.L., Chen, S., Zheng, A.H., 2005. The ion chemistry and the source of PM2.5 aerosol in Beijing. Atmospheric Environment 39, 3771–3784.
Wei, F.S., Chen, J.S., Wu, Y.Y., 1990. The Background Value of Soil Elements in China. China Environmental Science Press, Beijing.
Xia, D.S., Chen, F.H., Bloemendal, J., Liu, X.M., Yu, Y., Yang, L.P., 2008. Magnetic properties of urban dustfall in Lanzhou, China, and its environmental implications. Atmospheric Environment 42, 2198–2207.
Xie, S., Dearing, J.A., Bloemendal, J., 2000. The organic matter content of street dust in Liverpool, UK, and its association with dust magnetic properties. Atmospheric Environment 34, 269–275.
Xie, S., Dearing, J.A., Boyle, J.F., Bloemendal, J., Morse, A.P., 2001. Association between magnetic properties and element concentrations of Liverpool street dust and its implications. Journal of Applied Geophysics 48, 83–92.
Yang, X., Ding, Z., Fan, X., Zhou, Z., Ma, N., 2007. Processes and mechanisms of desertification in northern China during the last 30 years, with a special reference to the Hunshandake Sandy Land, eastern Inner Mongolia. CATENA 71, 2–12.
Yang, X., Zhu, B., Wang, X., Li, C., Zhou, Z., Chen, J., Yin, J., Lu, Y., 2008. Late Quaternary environmental changes and organic carbon density in the Hunshandake Sandy Land, eastern Inner Mongolia, China. Global Planet Change 61, 70–78.
Yang, Y.J., Wang, Y.S., Wen, T.X., Li, W., Zhao, Y.N., Li, L., 2009. Elemental composition of PM2.5 and PM10 at Mount Gongga in China during 2006. Atmospheric Research 93, 801–810.
Ye, D.Z., Chou, J.F., Liu, J.Y., 2000. Causes of sand-stormy weather in Northern China and contral measures. Acta Geographica Sinica 55, 513–521.
Zhang, J., Chen, Z.L., Wang, W., 1998. Source apportionment on fine particulate in atmosphere Beijing. Acta Science Circumstantiae 18, 62–67 (in Chinese with abstract in English).
Zhang, M.Q., Zhu, Y.C., Deng, R.W., 2002. Evaluation of mercury emissions to the atmosphere from coal combustion, China. AMBIO 31, 482–484.
Zhang, C.X., Liu, Q.S., Huang, B.C., Su, Y.L., 2010a. Magnetic enhancement upon heating of environmentally polluted samples containing haematite and iron. Geophysical Journal International 181, 1381–1394.
Zhang, X.X., Shi, P.J., Liu, L.Y., Tang, Y., Cao, H.W., Zhang, X.N., Hu, X., Guo, L.L., Lue, Y.L., Qu, Z.Q., Jia, Z.J., Yang, Y.Y., 2010b. Ambient TSP concentration and dustfall in major cities of China: spatial distribution and temporal variability. Atmospheric Environment 44, 1641–1648.
Zhang, C.X., Qiao, Q.Q., Piper, J.D.A., Huang, B.C., 2011. Assessment of heavy metal pollution from a Fe-smelting plant in urban river sediments using environmental magnetic and geochemical methods. Environmental Pollution 159, 3057–3070.
Zhang, C.X., Paterson, G.A., Liu, Q.S., 2012a. A new mechanism for the magnetic enhancement of hematite during heating: the role of clay minerals. Studia Geophysica Et Geodaetica 56, 845–860.
Zhang, C.X., Qiao, Q.Q., Appel, E., Huang, B.C., 2012b. Discriminating sources of anthropogenic heavy metals in urban street dusts using magnetic and chemical methods. Journal of Geochemical Exploration 119–120, 60–75.
Zhu, Z.D., Wu, Z., Liu, S., 1980. An Outline on Chinese Deserts. Kexue, Beijing.